Towards the Development of a Thyroid Ultrasound Biometric Scheme based on Tissue Echo-morphological Features

José C.R. Seabra[1,3] and Ana L.N. Fred[2,3]

[1] Institute for Systems and Robotics (ISR)
jseabra@isr.ist.utl.pt,
WWW homepage: http://users.isr.ist.utl.pt/~jseabra
[2] Institute of Telecommunications (IT)
[3] Instituto Superior Técnico (IST), Technical University of Lisbon, Lisbon, Portugal

Abstract. This paper proposes a biometric system based on features extracted from the thyroid tissue accessed through 2D ultrasound. Tissue echo-morphology, which accounts for the intensity (echogenicity), texture and structure has started to be used as a relevant parameter in a clinical setting. In this paper, features related to texture, morphology and tissue reflectivity are extracted from the ultrasound images and the most discriminant ones are selected as an input for a prototype biometric identification system. Several classifiers were tested, with the best results being achieved by a combination of classifiers (k-Nearest Neighbors, MAP and entropy distance). Using leave-one-out cross-validation method the identification rate was up to 94%. Features related to texture and echogenicity were tested individually with high identification rates up to 78% and 70%, respectively. This suggests that the acoustic impedance (reflectivity or echogenicity) of the tissue as well as texture are feasible parameters to discriminate between distinct subjects. This paper shows the effectiveness of the proposed classification, which can be used not only as a new biometric modality but also as a diagnostic tool.

1 Introduction

The thyroid is one of the largest endocrine glands in the body (see Fig.1). It controls how quickly the body burns energy, makes proteins and how sensitive the body should be to other hormones [15]. Thyroid ultrasonography is a non-invasive diagnostic exam, which provides immediate information on the structure and the characteristics of thyroid glands. This imaging modality is widely used in clinical practice because it combines low cost, short acquisition time, absence of ionizing radiations and sensitivity in ascertaining the morphology of the thyroid gland, as well as the size and number of thyroid nodules.

Ultrasound images usually present a low *signal to noise ratio* (SNR) and are characterized by a type of multiplicative noise called *speckle* that accompanies all coherent imaging modalities. It appears when images are obtained by

using coherent radiation and is the result of the constructive and destructive interference of the echoes scattered from heterogeneous tissues and organs [1].

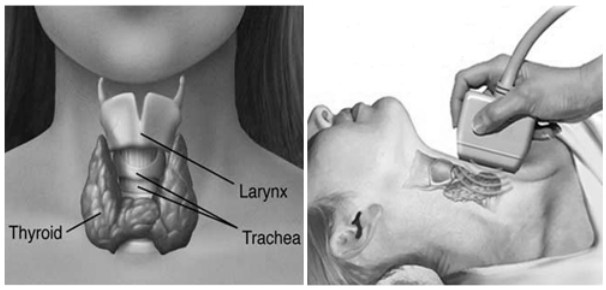

Fig. 1. Illustration of the thyroid gland's anatomy and location. An ultrasound examination is performed by placing the probe on the patient's neck (Courtesy of Mayo Foundation for Medical Education and Research).

The characteristic granular speckle pattern present in the ultrasound images makes the diagnostic task harder, whereas the subjectivity involved in their interpretation can be regarded as their major drawback. A framework which could provide explicit features extracted from the images would lead to a more reliable medical diagnosis, providing the experts with a second opinion and reducing the misdiagnosis rates.

Some studies have been developed which aim at characterizing the thyroid tissue using ultrasound image processing and analysis. Image intensity information has been used for the identification of thyroid Hashimoto disease [9], for the detection of nodular thyroid lesions, and for thyroid tumor classification. Textural image information encoded by means of co-occurrence matrix features [6] have been used for identification of chronic inflammations of the thyroid gland [14, 13] and for the discrimination between normal and pathologic tissues [4].

Tissue echo-morphology, which accounts for the intensity (echogenicity), texture and structure, has started to be used as a relevant parameter in a clinical setting (see Fig.2). Basically, features extracted from a given region, tissue or organ can be used to identify (classify) a patient as normal or as suffering from a pathological condition. In a classification context, this is considered to be a two-class problem.

This paper proposes a biometric system based on features extracted from the thyroid tissue accessed through 2D ultrasound. Biometrics deals with identification of individuals based on their physiological or behavioral characteristics. Identification (Who am I?) refers to the problem of establishing a subject's identity - either from a set of already known identities (closed identification problem) or otherwise (open identification problem) [7].

Thyroid tissue echo-morphology qualify to be a biometric because it is a universal feature, which means that every person has the characteristic, is distinct

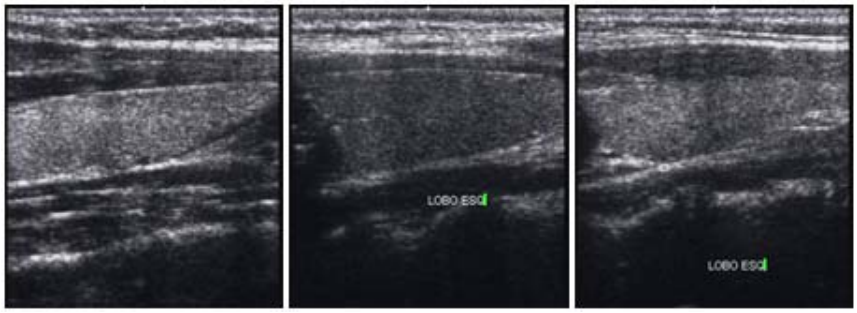

Fig. 2. Examples of thyroid ultrasound images, presenting different echo-morphologies. a) Hyperechogenic, b) Hypoechogenic and c) Heterogeneous thyroids.

from one individual to another, is permanent and can be easily collected through a common ultrasound scanner.

The paper is organized as follows. Section 2 formulates the problem and section 3 describes the feature module used in the biometric system. Section 4 presents the classifiers used in the identification problem. Section 5 presents the results obtained by the biometric system and section 6 concludes the paper.

2 Problem Formulation

In this paper, an analogy between two problems is made. In the context of medical diagnosis, a subject is assigned to one of two classes N (normal) or P (pathological). The risk of classifying pathological patients as normal (false negatives) should be penalized. Regarding a biometric identification problem, there is a class assigned to each individual. The maximum likelihood probabilities (or other types of scores) are computed in order to label the individual with its corresponding class.

The problem addressed in this paper can be stated as follows: given C_i classes, each corresponding to a different individual (registered in the database), and O_i observations, corresponding to 2D ultrasound sample images of the thyroid tissue recorded from each individual, establish the identity of new observations (label to the corresponding classes), which is a typical human identification problem.

The diagram block of the biometric system used in this paper is illustrated in Fig.3. It is mainly composed of three modules: (i) the sensor module, (ii) the feature extraction module, and (iii) the classification module.

The sensor module accounts for image acquisition. Ultrasound images of the thyroid gland were acquired longitudinally and transversally to the neck of 10 individuals, using an ultrasound scanner (Siemens Sonoline G50) operating in brightness (B-) mode. For each individual, the two lobes of the thyroid were scanned and one image per lobe was acquired. All thyroids were scanned under the same operating conditions in order to make the echo-morphological features extracted from the images independent of the scanner properties.

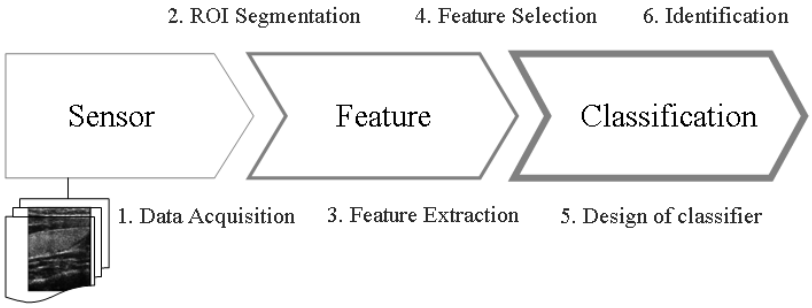

Fig. 3. Diagram block of the biometric identification system

3 Feature Extraction Module

The feature extraction module is an important part of the biometric system because it determines which features are used for identification. In this section it is also important to consider how the thyroid glands are segmented from the ultrasound images, which features qualify for individual characterization, and from those features which of them are more relevant for discriminating between classes (subjects).

3.1 Segmentation

Before extracting the relevant features that describe the echo-morphology of the thyroid glands it is important to segment its anatomy from the ultrasound images. This is an important step in the development of an automatic and robust biometric tool.

The thyroid glands are the regions of interest from where the features are to be extracted. This can be done by manually outline the contours of the thyroid, which is incredibly tedious and time-consuming.

One way to circumvent this problem is to use automatic or semi-automatic methods (Active Contours [17], Level Sets [16], Graph Cuts [2, 8]). In this paper, a semi-automatic method based on Gradient Vector Flow (GVF) active contours (snakes) is used.

Active contours [17], or snakes, are computer-generated curves that move within images to find the boundaries of the region of interest. The GVF snake begins with the calculation of a field of forces, called the GVF forces, over the image domain. The GVF forces are used to drive the snake, modeled as a physical object having a resistance to both stretching and bending towards the boundaries of the object. The GVF forces are calculated by applying generalized diffusion equations to both components of the gradient of an image edge map (see Fig.4). The semi-automatic nature of the segmentation process is due to user-dependent initialization: in fact, to make the method more robust, the user should provide a rough initialization of the contour by giving some initial clicks on the image.

3.2 Feature Extraction

After obtaining the segmented thyroid glands, 6 rectangular windows (32 by 32 pixels) were extracted from each lobe and were used for training. Similarly, 3 other regions were also extracted (see Fig.5) and used for testing.

Three different types of features are then computed for each rectangular window: (i) 2 features associated with the Rayleigh distribution parameter, (ii) 4 wavelet energy coefficients, (iii) 4 radon transform parameters. These features are also combined with the longitudinal mid-distance measure for each thyroid gland. This distance corresponds to the vertical distance measured between the borders of the thyroid at its middle section. In summary, 11 features are used to characterize each sample taken from the segmented thyroids.

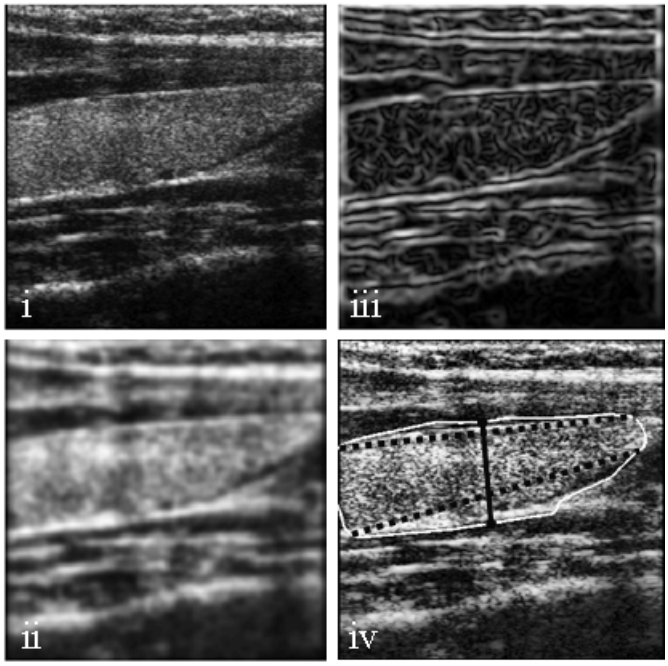

Fig. 4. Semi-automatic segmentation using GVF active contours: (i) original image, (ii) image convolved with gaussian mask, (iii) image edge map, (iv) segmented thyroid (the extraction of the mid-distance measure is also shown).

3.3 Rayleigh distribution parameters from original sample and speckle field

The speckle pattern present in the ultrasound images is a result of the interference of echoes at the surface of the transducer, which emanate from the acoustic impedance of the tissues.

Several statistical models are proposed in the literature to describe this kind of pattern [10]. One of the most used in ultrasound (US), LASER and *Synthetic Aperture Radar* (SAR) is the Rayleigh distribution [3]. Commonly the speckle pattern is called speckle noise, and is often studied in de-noising problems. Another view of the problem, which is considered in this paper, is to accurately reconstruct the ultrasound images to provide a measure of the local acoustic impedance of the tissues.

In this context, a bayesian reconstruction method with a log-Euclidean prior is used [12]. In this approach, the ill-poseness nature of the reconstruction (de-noising) problem is circumvented by using *a priori* information about the unknown image to be estimated. The estimation is formulated as an optimization task where a two-term energy function is minimized. The first term pushes the solution toward the observations and the second regularizes the solution.

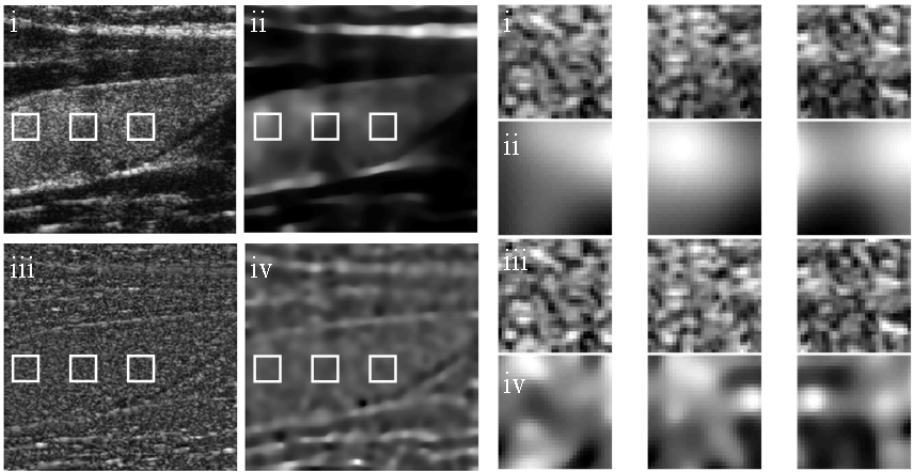

Fig. 5. (Left) (i) Original image, (ii) reconstructed image (local rayleigh parameters), (iii) Speckle field, and (iv) Rayleigh estimation of the speckle field. (Right) Illustration of samples used for testing (i) and their corresponding Rayleigh estimates, speckle field and Rayleigh estimation of the speckle field (ii, iii and iv).

Let $X = \{x_{i,j}\}$ and $Y = \{y_{i,j}\}$ be a $N \times M$ image presenting the acoustic impedance of the tissue and a speckle image, respectively. The *speckle* pattern of the image $Y = \{y_{i,j}\}$ is described by a Rayleigh distribution,

$$p(y_{i,j}|x_{i,j}) = \frac{y_{i,j}}{x_{i,j}} e^{-\frac{y_{i,j}^2}{2x_{i,j}}}. \tag{1}$$

The estimation of X from Y is formulated as the following optimization task

$$\hat{X} = \arg\min_X E(X, Y), \tag{2}$$

where $E(X,Y)$ is an energy function.

The optimization problem, described by equation (2), is usually *ill-posed* in the Hadamard sense. This difficulty may be overcome by using the *maximum a posteriori* (MAP) criterion,

$$E(X,Y) = \underbrace{E_Y(X,Y)}_{\text{data fidelity term}} + \underbrace{E_X(X)}_{\text{prior term}}, \tag{3}$$

where $E_Y(X,Y)$, called *data fidelity term*, is the symmetric of the log-likelihood function

$$E_Y(X,Y) = -\log\left[\prod_{i,j=1}^{N,M} p(y_{i,j}|x_{i,j})\right], \tag{4}$$

where it is assumed statistical independence of the observations [5].

The solution to this problem (in fact, an energy minimization problem) is an image (see Fig.5 (ii)) in which the value of each pixel is the Rayleigh parameter that characterizes accurately the local reflectivity of the tissue being scanned. Thus, for each sample, one Rayleigh distribution parameter is extracted by averaging the local Rayleigh parameters inside the sampled window.

Moreover, it is known that the speckle corrupting the ultrasound images is multiplicative in the sense that its variance depends on the underlying estimated signal X. The image formation model may be formulated as follows: $Y = \eta\sqrt{X}$ where X is the noiseless image and η is the corresponding noise intensity (see Fig.5 (iii)). A similar reconstruction procedure was performed to extract one Rayleigh distribution parameter associated with the speckle field of each sample (see Fig.5 (iv)). The speckle field is used in the sequel of the paper to extract different textural features.

3.4 Wavelet energy coefficients

Texture information is hypothesized as being a relevant parameter to discriminate between thyroids and therefore individuals. One way to assess the texture of a given sample is to decompose its corresponding speckle field using 2D wavelets (see Fig.6(iii)). This kind of decomposition consists in using low and high pass filters onto the approximation coefficients at level j (the original image) in order to obtain the approximation at level j+1, and the details in three orientations (horizontal, vertical, and diagonal). This method is performed along 3 levels. Every subimage contains information of a specific scale and orientation, which is conveniently separated. The amount of detail for each resolution level, which accounts for the level of heterogeneity in each sample being studied, is computed as the sum of horizontal, vertical and diagonal detail energies for each level. Therefore, in this paper each sample will be also described by one feature accounting for the approximation energy as well as three different detail energies.

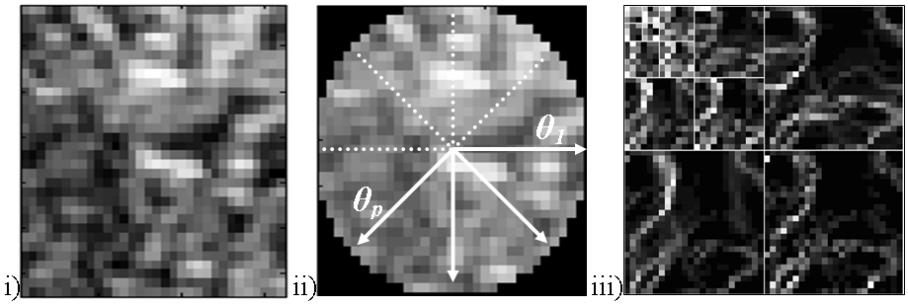

Fig. 6. Wavelet decomposition. Multi-resolution texture is assessed through the detail energy levels.

3.5 Radon transform features

In this paper, it is also hypothesized that the thyroid tissue may be characterized by different directionality patterns observed in the ultrasound images. The encoding of the directional patterns is realized by means of Radon Transform features [11]. The idea is to project the image intensity along a radial line oriented at different angles (0, 45, 90 and 135 degrees).

Let (x, y) be the cartesian coordinates of a point in a 2D image, and $u(x, y)$ the image intensity. Then, the 2D radon transform denoted as $R_u(\rho, \theta)$ is given by

$$R_u(\rho, \theta) = \int_{-\infty}^{+\infty} \int_{-\infty}^{+\infty} u(x, y)\delta(\rho - xcos\theta - ysin\theta)dxdy \tag{5}$$

where ρ is the perpendicular distance of a line from the origin and θ is the angle formed by the distance vector. The feature vector can be defined as

$$F = [\sigma([R_{u_1}(\rho, \theta_1)..., R_{u_n}(\rho, \theta_1)]), ..., \sigma([R_{u_1}(\rho, \theta_p), ..., R_{u_n}(\rho, \theta_p)])], \tag{6}$$

where $\sigma = \frac{R_u(\rho,\theta)}{u(x,y)}$ accounts for the contribution of the radon transform along four distinct angles $\theta_i = \{0, 45, 90, 135^o\}$.

3.6 Dimensionality reduction

At this point, 11 features per sample (each sample corresponding to a rectangular window) were extracted: 2 features associated with the Rayleigh distribution, 1 mid-distance measure, 4 wavelet energies, and 4 radon transform parameters. The amount of features extracted (11 features per sample, 6 samples per thyroid lobe, 2 lobes per individual, 10 individuals) makes the identification problem a complex task.

One way to deal with this problem and to eliminate the redundancy among features is to use principal component analysis (PCA). This approach is used to better handle and visualize the data by selecting the 3 most discriminating axis in the feature space and computing the 3 most relevant features (projection of the observations onto these axis). In summary, 3 features (components of the PCA) per observation sample are used in the identification problem. Fig.7(i) shows the representation of the observations (each individual sample) in the new feature space, where the 3 components of the PCA represent the 3 dimensions of the plot.

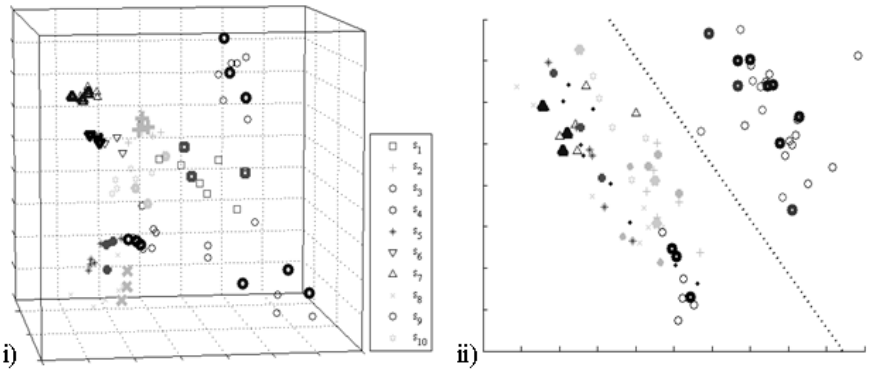

Fig. 7. Feature selection using PCA. (i) Representation of the observations (6 samples per individual) in the new PCA-derived feature space. Training samples (belonging to different classes) are represented with light symbols while testing samples are shown in bold. (ii) 2D feature space, showing a clear discrimination of the observed samples into two classes (gender of subjects)

This new PCA-derived feature space can be projected onto a 2 dimensional feature space. Fig.7(ii) shows that the 2D features are able to clearly discriminate between two groups of individuals: one class addressed to men and the other to women. Even though no prior information is known about the clinical status of the individuals subject to this test it is clearly suggested that echo-morphology information might be correlated with the different types and quantities of hormones produced by men and women. This fact can lead to thyroids presenting different acoustic impedances and textures. This also explains the good discrimination between male and female populations.

At this point, we can suggest that this system might be useful as a soft biometric system for gender identification.

4 Classification Module

In this paper, a closed set identification problem is addressed, which means that N possible outputs are generated for N possible models. The decision on whether to classify an observation (individual features) as being part of any of the available classes (individual database) is based on a computed score (MAP probability, distance measure, entropy). Three types of classifiers were studied:

4.1 K-Nearest neighbors classifier

The K-Nearest neighbors (KNN) classifier is based on the idea that an object is classified by a majority vote of its neighbors, with the object being assigned to the class most common amongst its k nearest neighbors. This is a common nonlinear classifier which results, when 1NN is used, in a Voronoi tesselation of the feature space.

4.2 MAP classifier

The Maximum a Posteriori classifier is based on the MAP probability of a class ω given an observation X

$$\hat{\omega} = \arg\max p(\omega|X). \tag{7}$$

In our work we assume that the observations can be modeled by a multivariate gaussian distribution given by

$$p(X, \mu, \Sigma) = \frac{1}{2\pi^{3/2}|\Sigma|^{1/2}}\, e^{-1/2(X-\mu)'\Sigma^{-1}(X-\mu)}. \tag{8}$$

In this framework the discriminant function to be maximized is given by

$$g_i(X) = \log p(X|\omega_i) + \log p(\omega_i) \tag{9}$$

where $g_i(X) = -\frac{1}{2}\log|\Sigma_i| - \frac{1}{2}(X-\mu_i)'\Sigma_i(X-\mu_i) + \log p(\omega_i)$, and μ_i and σ_i are maximum likelihood estimates of the mean and covariance matrices of the pdf of class i, based on the training data; $p(\omega_i) = 1/N$, being N the number of individuals in the database.

4.3 Minimum entropy distance classifier

As it was described before, the underlying observation model for each sample is described by a Rayleigh parameter (reflectivity) (see Fig.8(i)). The approximated probability density function (PDFs) generated using this Rayleigh parameter can be compared with the other PDFs in the database (Fig.8(ii)).

Conformity tests using the PDF for a given individual (testing distribution) and the remaining PDFs from the database (training distributions) were performed in order to assess which distribution better represents the observed one.

Considering the Kolmogorov-Smirnov conformity statistical test, $P_e = 1 - P_{H_0}$ is the probability of rejecting the null hypothesis, H_0, which is the hypothesis of the data have been generated by any of the distributions from the database. Here, $P_{H_0} = Q_{KS}(\lambda)$, $Q_{KS}(\lambda) = 2\sum_{j=1}^{\infty}(-1)^{j-1}e^{-2j^2\lambda^2}$, $\lambda = (\sqrt{(}N) + 0.12 + \frac{0.11}{\sqrt{N}})\,D$, N is the number of data points and $D = max|c(n) - ch(n)|$, where $c(n)$ and $ch(n)$ are the cumulative probability functions of the testing and training distributions.

The Kullback-Leibler entropy distance is given by, $d = \sum_n p(n)\,log(\frac{p(n)}{h(n)})$. Here, $p(n)$ is the training distribution and $h(n)$ is the histogram of the observed (testing) sample.

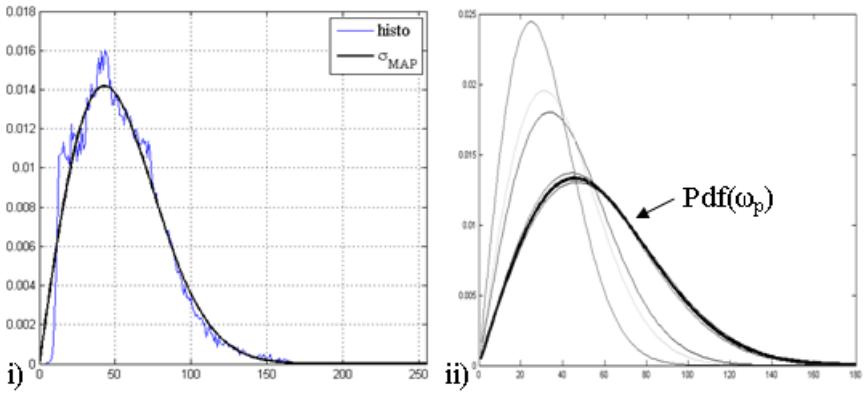

Fig. 8. The histogram of an observed sample can be approximated by a Rayleigh distribution with an estimated parameter which accounts for the acoustic impedance of the sample tissue. This distribution can be compared with the others in the database and entropy distance measures can be computed.

The aforementioned classifiers were used individually but also in a combined scheme. The idea is to put together the classification given by each classifier and use a voting strategy to yield a final classification for each sample.

5 Results and Discussion

The performance of the classifiers was tested through 2 experiments and the result is summarized in Table 1. In the first experiment, 60 samples from one thyroid lobe were used as training data and 30 samples from the same lobe were used as testing data. The second experiment uses training data from one thyroid

Table 1. Performance of the classifiers (k-nNeighbors, MAP, SmirKolm, KullLeibler, and combination of the mentioned classifiers) for two different data samples, using all the features available, only textural features and features computed by PCA. These results refer to average values of identification rates as well as standard deviations, obtained through 10 consecutive runs of the classification methodology. Results achieved with the Leave-One-Out method are also shown.

	Identification Rate		
Classifier	Features	Exp.1	Exp.2
k-nNeigh	All	0.858 ± 0.117	0.222 ± 0.051
	PCA	0.878 ± 0.100	0.267 ± 0.050
	Texture	0.789 ± 0.150	0.233 ± 0.088
MAP	All	0.400 ± 0.100	0.300 ± 0.111
	PCA	0.822 ± 0.154	0.656 ± 0.256
	Texture	0.722 ± 0.050	0.456 ± 0.077
SmirKol	Rayleigh	0.700 ± 0.067	0.211 ± 0.039
kullLeib	Rayleigh	0.700 ± 0.067	0.211 ± 0.039
Combined	All	0.878 ± 0.069	0.674 ± 0.084
	PCA	0.922 ± 0.069	0.756 ± 0.184
Combined clssf. w/ LeaveOneOut	PCA	0.937 ± 0.099	0.948 ± 0.175

lobe (60 samples) and testing data from the opposite lobe (30 samples). Regarding the k-nearest neighbor and the MAP classifiers, tests were performed considering (i) all the features available, (ii) only the ones corresponding to the Radon transform and wavelets, which account for texture information, and (iii) the PCA derived features. The conformity tests (Kolmogorov-Smirnov, Kullback-Leibler) consider only the Rayleigh parameter (acoustic impedance or reflectivity) as describing each sample. The combined classifier was tested with all the features available as well as with the ones obtained after PCA.

In order to make the classification scenario as reliable as possible 10 runs of classification were performed, where in each run different thyroid samples were selected from the images. The identification rates shown in Table 1 are averaged values of the identification rates obtained for each run of classification.

The best performance is achieved by using a combination of all the mentioned classifiers, considering the PCA derived features, with high correct identification (ID) rates for both experiments (ID rate for Exp.1 = 0.922±0.069 and for Exp.2 = 0.756±0.184). When all the features are considered by the combined classifier, ID results are also reasonably good.

The ID rates obtained both with MAP and the K-Nearest neighbors classifier using only textural features were also high, which allows to conclude that texture information is in fact relevant for tissue characterization and differentiation. Textural features have already been shown to be relevant in a similar context [13]. The poor performance of these classifiers for Exp.2 when using these kind of features suggests that textural contents change significantly from one thyroid lobe to the other.

A good performance is also achieved with the entropy distance classifiers (KullLeib and SmiKol) for the first data set (Exp.1). This suggests that the acoustic impedance of the thyroid tissue (which is the only parameter used by these two classifiers) is indeed a good parameter for discriminating between thyroids and thus individuals. The poor performance of these classifiers when using the second data set suggests once more that the echo-morphology varies significantly from one thyroid lobe to the other.

Thus, it appears that textural and echogenicity features strongly vary from one lobe to another and therefore in order to improve the effectiveness of using echo-morphological features in both a clinical and a biometric setting, only one lobe of the thyroid should be considered for study.

Another estimate of the accuracy of the classifier uses the leave-one-out method. In this case, all but one sample from each lobe (Exp.1) or from both lobes (Exp.2) were used, thus using a larger training data set. Again, the combined classifier was used because it was the one which achieved better results in the previous experiment. Again, considering Table 1 it is observed a good performance of the classifier, in which the classifier even outperforms for Exp.2 (ID rates for Exp.1: 0.937 ± 0.099 and Exp.2: 0.948 ± 0.175). This suggests that the number of samples in the database significantly affects the performance of the classifier.

6 Conclusions

Computer derived features from 2D ultrasound images of the thyroid glands were used as part of a prototype biometric system. These features are related to the acoustic impedance, texture and morphology of the thyroid tissue.

Good results were achieved with all the classifiers used individually but the best performance was obtain with a combination of all the classifiers when using the three most discriminant features, computed by PCA. Moreover, reasonably high identification rates were also achieved with the entropy distance classifiers considering the Rayleigh distribution parameter, suggesting that the acoustic impedance, or reflectivity, of the tissues is a relevant feature to discriminate between individuals. Similarly, good performance was achieved when textural features computed from the speckle field were considered, which allows to conclude that the speckle field has important textural content. Analysis of thyroid echo-morphology should be further exploited because it appears to be very useful not only as a (soft) biometric system but also as a diagnostic tool.

Preliminary results, using 11 parameters extracted from ultrasound images, are encouraging. Further studies, involving larger data sets (more individuals and more samples), as well as observations taken from multiple sessions along distinct time instants, are required to better establish the accuracy of this new biometric modality.

Acknowledgments The authors would like to thank Dr. Ricardo Ribeiro, from Escola Superior de Tecnologia de Saúde de Lisboa, for his help in performing the ultrasound scans and providing the thyroid images.

References

1. J. Abbot and F. Thurstone. Acoustic speckle: Theory and experimental analysis. *Ultrasound Imaging*, 1:303–324, 1979.
2. Y. Boykov, O. Veksler, and R. Zabih. Fast approximate energy minimization via graph cuts. *IEEE Trans. Pattern Anal. Mach. Intell.*, 23(11):1222–1239, 2001.
3. C. Burckhardt. Speckle in ultrasound b-mode scans. *IEEE Transations on Sonics and Ultrasonics*, SU-25(1):1–6, January 1978.
4. S. Catherine, L. Maria, A. Aristides, and V. Lambros. Quantitative image analysis in sonograms of the thyroid gland. *Nuclear Instruments and Methods in Physics Research A*, 569:606–609, December 2006.
5. J. Dias, T. Silva, and J. Leitão. Adaptive restoration of speckled SAR images using a compound random markov field. In *Procedings IEEE International Conference on Image Processing, Vol.II*, pages 79–83, Chicago, USA, October 1998. IEEE.
6. R. M. Haralick, Dinstein, and K. Shanmugam. Textural features for image classification. *IEEE Transactions on Systems, Man, and Cybernetics*, SMC-3:610–621, November 1973.
7. Flynn P. Jain A.K. and Ross A.A. Handbook of biometrics, Springer 2008.
8. V. Kolmogorov and R. Zabih. What energy functions can be minimizedvia graph cuts? *IEEE Trans. Pattern Anal. Mach. Intell.*, 26(2):147–159, 2004.
9. Guy Mailloux, Michel Bertrand, Robert Stampfler, and Serge Ethier. Computer analysis of echographic textures in hashimoto disease of the thyroid. *Journal of Clinical Ultrasound*, 14(7):521–527, 1986.
10. O. V. Michailovich and A. Tannenbaum. Despeckling of medical ultrasound images. *IEEE Transactions on Ultrasonics, Ferroelectrics and Frequency Control*, 53(1):64–78, 2006.
11. M.A. Savelonas, D.K. Iakovidis, N. Dimitropoulos, and D. Maroulis. Computational characterization of thyroid tissue in the radon domain. *Computer-Based Medical Systems, 2007. CBMS '07. Twentieth IEEE International Symposium on*, pages 189–192, June 2007.
12. José Seabra, João Xavier, and João Sanches. Convex ultrasound image reconstruction with log-euclidean priors. In *In Proc. of the Engineering in Medicine and Biology Conference*, Vancouver, Canada, 2008.
13. Daniel Smutek, Radim Sara, Petr Sucharda, and Ludvik Tesar. Different types of image texture features in ultrasound of patients with lymphocytic thyroiditis. In *ISICT '03: Proceedings of the 1st international symposium on Information and communication technologies*, pages 100–102. Trinity College Dublin, 2003.
14. Daniel Smutek, Radim Sara, Petr Sucharda, and Ludvik Tesar. Image texture analysis of sonograms in chronic inflammations of thyroid gland. *Ultrasound in Medicine and Biology*, 29:1531–1543(13), November 2003.
15. Tortora Gerard J Tortora, Gerard J. (Gerard Joseph). Principles of anatomy and physiology, 2000.
16. C. M. van Bemmel, L. Spreeuwers, M.A. Viergever, and W.J. Niessen. Level-set based carotid artery segmentation for stenosis grading. In *MICCAI '02: Proceedings of the 5th International Conference on Medical Image Computing and Computer-Assisted Intervention-Part II*, pages 36–43, London, UK, 2002. Springer-Verlag.
17. C. Xu and J.L. Prince. Snakes, shapes, and gradient vector flow. *IEEE Transactions on Image Processing*, 7(3), March 1998.